

NUMERICAL ANALYSIS OF RESPONSE OF PLATE ANCHOR UNDER COMBINED LOADING

Md. Al-Amin¹, Md. Shafiqul Islam², Mst. Rahanuma Tajnin³, Grytan Sarkar⁴ and Md. Rokonuzzaman⁵

¹Undergraduate Student, Dept. of Civil Engineering, Khulna University of Engineering & Technology, Khulna, Bangladesh, e-mail: ashik.ghs@gmail.com

²Assistant Professor, Dept. of Civil Engineering, Khulna University of Engineering & Technology, Khulna, Bangladesh, e-mail: shafiq0837@gmail.com

³Assistant Engineer, Public Works Department (PWD), Division-2, Khulna, Bangladesh, e-mail: rtajnin@gmail.com

⁴Assistant Professor, Dept. of Civil Engineering, Khulna University of Engineering & Technology, Khulna-9203, Bangladesh, e-mail: grytan_ce04@yahoo.com

⁵ Professor, Dept. of Civil Engineering, Khulna University of Engineering & Technology, Khulna, Bangladesh, e-mail: rokoncekuet@yahoo.com

ABSTRACT

Drag anchor is an economical foundation option, although its installation procedure is not understood properly. For this reason, it is necessary to define failure envelope and failure mechanism of anchor soil under combined loading. The present study focuses on the capacity of drag anchor under uni-directional vertical, horizontal and moment loading in homogeneous clay deposit. A model of deeply embedded strip anchor exposed to combined loading is analyzed by two-dimensional finite element analysis (FEA) based on swipe and probe test procedure. Numerical result reveals that the failure envelope of swipe test procedure lie inside the true failure envelope of probe test under combined loading. For normal loads lower than 45% of ultimate vertical load, parallel loading as well as moment loading, dominate the failure mechanism of the plate anchor. Moreover, in this study, some remarkable soil failure mechanisms under combined loading are produced.

Keywords: Finite element analyses (FEA), drag anchor, combined loading and failure envelope.

1. INTRODUCTION

Offshore structure and their foundation system are usually subjected to large vertical, horizontal load and overturning moment due to the movement of wind, wave and many other environmental loadings. Floating structures anchored to the seabed using catenary and taut-wire mooring systems are generally more technically feasible and cost effective than gravity-based platforms in these deep-water environments. Drag anchor is used widely due to its simplicity to design high economic value, low cost of installation and high pullout capacity relative to the low anchor weight in soft clay (Kim 2007). Hence, the anchor final position is important because it determine the anchor holding capacity. But, there are lot of vagueness of the anchor position during and after the installation and still a major problem for anchor design. Therefore, it is necessary and important to understand the anchor behaviour correctly during installation. The method using yield envelopes to characterize the anchor behaviour under combined loading for installation prediction is promising. This method has been used for the installation behaviour prediction of the drag embedment anchor (DEA) and vertical loaded anchor (M P O'Neill et al., 2003;Elkhatib and Randolph, 2005; Yang, et al., 2010) the prediction of keying process of suction embedded plate anchor (SEPLA) and OMNI-MAX anchor (Aubeny et al., 2008;Yang et al., 2011;Cassidy et al. 2012;Tian et al.,2012; Wei et al., 2015; Liu et al., 2016).

Due to the complex geometry of practical drag anchors, studies on drag anchors usually start from anchor plate with simplified geometry, which is similar to plate anchor. The majority of the earlier studies have focused on the plate anchor uplift capacity, which is based on analytical solutions or experimental data. Numerical studies have been conducted by (Rowe, 1978; Merifield et al., 2003; Song and Hu, 2005; Song et al., 2008 and Wang et al., 2009). However, these studies are focused only the vertical pullout capacities of plate anchor. But, the anchor plate subjected to combined vertical, horizontal and moment loading. In order to recognize the behaviour anchor plate under combined loading and analyse the failure pattern, it is essential to recognize the anchor behaviour under combined vertical, horizontal and moment loading or combination of all three. The controlling values of anchor capacity under the three uni-directional loadings with deep localized failure were studied by O' Neill et al. (2003), Elkhatib and Randolph (2005), Elkhatib (2006) and Wu et al. (2017).

In order to solve the above problems and to understand the correct failure mechanism, the present study emphasizes on the drag anchor capacity under pure vertical, horizontal and moment loading and combination of any of two loadings. The trajectory prediction using yield envelopes in current studies assumed deep anchor behaviour for the whole drag process by using yield envelope for deep anchor behaviour. Detailed analyses of swipe and probe tests are conducted to understand the behaviour of anchor under combined loading. In order to understand the failure mechanism in horizontal-moment loadings load-displacement probe tests are conducted.

2. METHODOLOGY

2.1 Finite Element Model

The objectives of this study are to improve the understanding of the fundamental mechanism of continuous pullout of horizontal anchor under combined loading condition of V, H and M. In this study, the two-dimensional finite element analysis (FEA) is carried out by commercial software ABAQUS. The strip plate anchor of width B is assumed to be deeply embedded, with localized plastic flow forming around the plate anchor and not extending to the surface, resulting in capacity factors that are not affected by overburden and soil weight (Song et al., 2008; Wang et al. 2010). Conventional small strain analysis is carried out to determine the pullout capacity of embedded anchor, where the anchor movement is limited to 0.1 times to the anchor length. The contact between the anchor and the soil is assumed to be fully bonded. In order to ensure the fully bonded condition, the interfaces between the anchor plate and soil domains are defined as (i) tangential behaviour and (ii) normal behaviour. In tangential behaviour is assumed to be rough and normal behaviour is defined as hard contact with no separation between soil and anchor when tension develops. An elastic perfectly plastic associative Mohr-Coulomb material model is used for purely cohesive soil with cohesion $c=10$ kPa, modulus of elasticity $E=10$ Mpa and the Poisson's ratio 0.49. The anchor is modelled as rigid body with young's modulus 10^7 times that of soil and Poisson's ratio 0.15 (Andersen et al., 2003). The FE analyses are based on 4-noded linear hybrid elements of type CPE4H. Figure 1 presents a typical two-dimensional finite-element mesh for a strip plate of width $B=0.5$ m and thickness $t=L/7=0.071$ m. The soil domain is extended to $20B$ in horizontal and vertical directions, respectively. Zero-displacement boundary conditions are applied to prevent out-of-plane displacements of the vertical boundaries and the base of the mesh is fixed in both horizontal and vertical coordinate directions. To obtain more accurate results, elements are kept very small ($L/60$) near the plate, increasing gradually in size and moving away from the plate (Nouri et al., 2017).

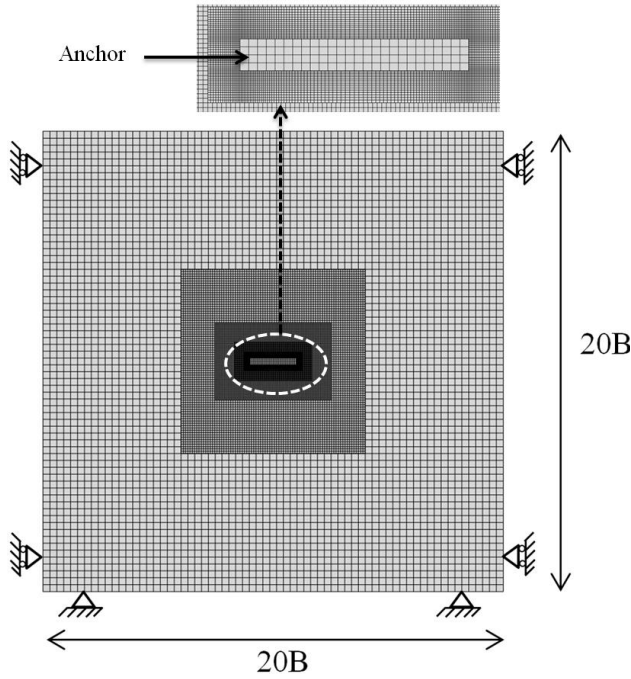


Figure 1: Finite element model used for numerical analysis

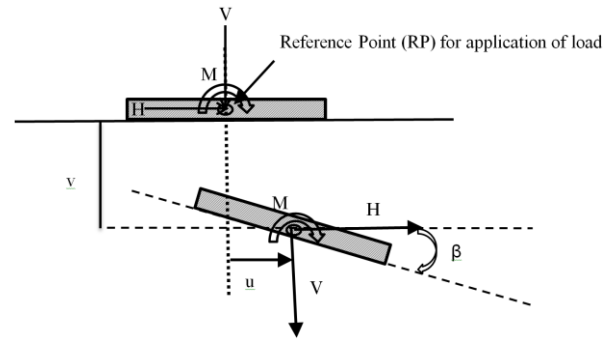


Figure 2: Load and displacement convention adopted

To determine the collapse load of the anchor, displacement-based analyses are performed. The total displacement is applied over a number of sub-steps in the reference point (RP) of anchor as shown in Figure.2. All the nodes defining the soil anchor interfaces are forced to move together either parallel to the anchor (sliding), perpendicular to the anchor (normal) and in a path corresponding to rotation of anchor plate about the centre. All results are presented here as non-dimensional forms using the factors defined as

$$N_v = \frac{V}{Bc}; N_s = \frac{H}{Bc}; N_m = \frac{M}{B^2c} \quad (1)$$

Where H, V and M are the normal, parallel and rotational capacities (normal to the intended plane of loading), respectively.

2.2 Sign Convention for Load and Displacement

The centroid of anchor is used as the reference point (RP) for application of combined load components V, H and M. The notation used in this paper is shown in Figure.2. The V, H and M loads as well as the corresponding footing movements' v, u and β are also illustrated in Figure. 2. The sign convention for loads presented and displacements in this study obeys a right-handed rule and clockwise positive convention as proposed by Butterfield and Houlsby (1997). The anchor's ultimate pullout capacities for pure loading of one single component (i.e. for ultimate pure moment load capacity $V=H=0$), are de-noted as V_0 , H_0 and M_0 for pure vertical, horizontal and moment loadings, respectively.

2.3 Numerical Analysis to Define the Failure Envelope

In the finite element analysis (FEA), the load is usually applied in two ways such that load-controlled method and displacement-controlled method. The benefit of displacement-controlled method is to simulate post failure phenomena's. From the load displacement response of anchor in any direction it can be concluded that the anchor is in limit equilibrium state in that direction. In this state, the slope of load displacement curve is tends to zero that means loads does not increase with the increase of load. It indicates that the ultimate load capacity (H, V and M) of anchor in that direction (v, u and β). For combination of load the

displacement controlled method is found to be more suitable instead of load controlled method (Bransby and Randolph, 1997). Constant-ratio displacement probe tests and displacement-controlled swipe tests were carried out to determine the post failure phenomena's in different loading planes, such as vertical horizontal plane (V:H, where $V>0$, $H>0$ and $M=0$), vertical moment plane (V:M, where $V>0$, $M>0$ and $H=0$) and horizontal moment plane (H:M, where $H>0$, $M>0$ and $V=0$).

2.3.1 Swipe test

The sideswipe test was first introduced by Tan (1990) during centrifugal modelling in sand. Many researchers have used frequently this test procedure in both experimental (Houlsby, 1994; Martin and Houlsby, 2001, Cassidy et al., 2002 and numerical (Bransby and Randolph, 1998; Gourvenec and Randolph 2003; Yang et al., 2010 and Randolph et al., 2011) studies.

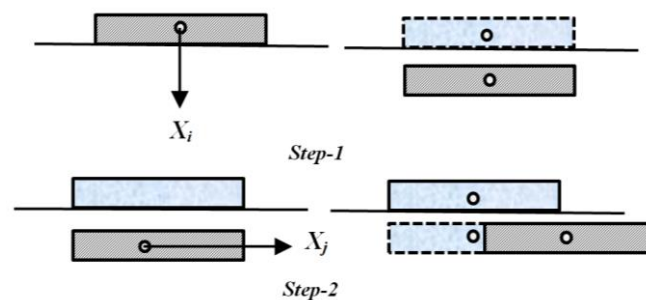


Figure 3: Example of a swipe test

Swipe tests are carried out to identify the failure envelopes in VH and VM plane, but are unsuitable for loading in the HM plane (Bransby et al., 2003). For a failure envelope in ij plane a displacement X_i is applied at the RP along i -direction from zero load state to limit equilibrium state at which ultimate load in that direction is reached. In its second step a displacement X_j is imposed in j -direction keeping constant displacement in i -direction displacement until the anchor load does not vary with the increased displacement in j -direction. The benefit of the swipe test is that a complete failure locus on a certain plane can be determined in a single test. The resultant load path is the failure envelope in ij -plane.

2.3.2 Probe analysis

Fixed displacement ratio probe test suggested by Bransby and Randolph (1997) is another way to check the accuracy of the failure envelopes obtained from the swipe tests. The probe tests give rise to load paths that move from the origin across the failure envelope, initially at gradients determined by the elastic stiffness but with the gradients changing owing to internal plastic yielding as the paths approach the failure envelope. Once the failure envelope is reached, each loading path travels around the failure envelope until it reaches a termination point where the direction of tangent to the failure envelope matches with the prescribed displacement ratio. However, several analyses with different displacement ratio are required to define the correct failure loci, it defines correct failure envelope specially in H:M loading plane. Fig. 4 shows the load paths for twenty $D\beta/Du$ displacement ratios ($v=0$) and final termination point agrees well with the failure envelope.

3. RESULTS AND DISCUSSION

One combination of V , H and M loads causing anchor to failure is found by translating and/or rotating the anchor until a constant load state is reached in that direction. The crudest example of this is to push the anchor in vertical direction into the soil until the vertical load plateaus reached is followed by translating and/or rotation. However, to define a complete failure envelope in different plane a variety of vertical and horizontal displacement and

rotational combinations are required. In this study, total 40 probe tests were conducted to define failure envelope in three different planes. The failure envelopes in the V–H, V–M and H–M planes are found by connecting the termination points. A summary of dimensionless normal, shear and rotational capacities of anchor under pure loading is provided in Table 1.

Table 1: Bearing Capacity Factors

Bearing capacity factors	Current FEM study	API/Deepstar
$N_{v0}=V_{ult}/Bc$	11.98	11.58
$N_{s0}=H_{ult}/Bc$	4.39	4.49
$N_{m0}=M_{ult}/B^2c$	1.63	1.74

The capacity factors shown in Table 1 are compared with the API/Deepstar study (Andersen et al., 2003). Current FEM study agreed well with the API/Deepstar study. The pure normal capacity (N_{v0}) of current FEM are found 3%, higher than that of API/Deepstar study. But, pure shear (N_{s0}) and pure moment (N_{m0}) capacities are found 2% and 6%, respectively. These slight disagreements might be due to different mesh configurations and other minor details of the model.

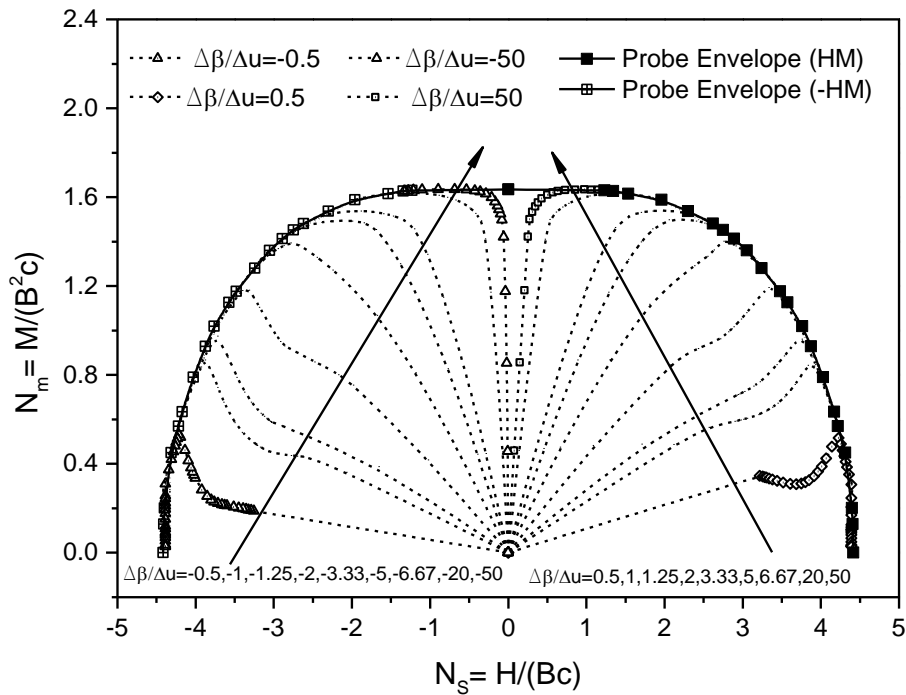


Figure 4. Loading path and failure envelope at H-M plane ($V=0$)

The failure envelopes for H:M loading shown in Figure. 4 is obtained from the 10 different probe tests for both HM and –HM failure. Different displacement ratios ranging from 0.5 to 50 are considered to construct complete failure envelope for both HM and –HM planes. The envelopes are symmetric, with the maximum moment $M_{max} = 1.63$ at $H=0$. At a lower shear loading upto $0.45H_{ult}$, the slope of HM failure envelope is almost zero. After that, it changes abruptly and slope of the failure envelope is found to be steeper at lower value of moment. Hence, it can be concluded that at a lower shear loading moment loading dominates the failure mechanism. The Figure.5 shows the comparison of failure envelope with the previous studies (Andersen et al., 2003 and Yang et al., 2010). The solutions obtained in the present study are in good agreement with a research conducted by Yang et al. (2010), but small discrepancies upto 6% are found with the API/Deepstar.

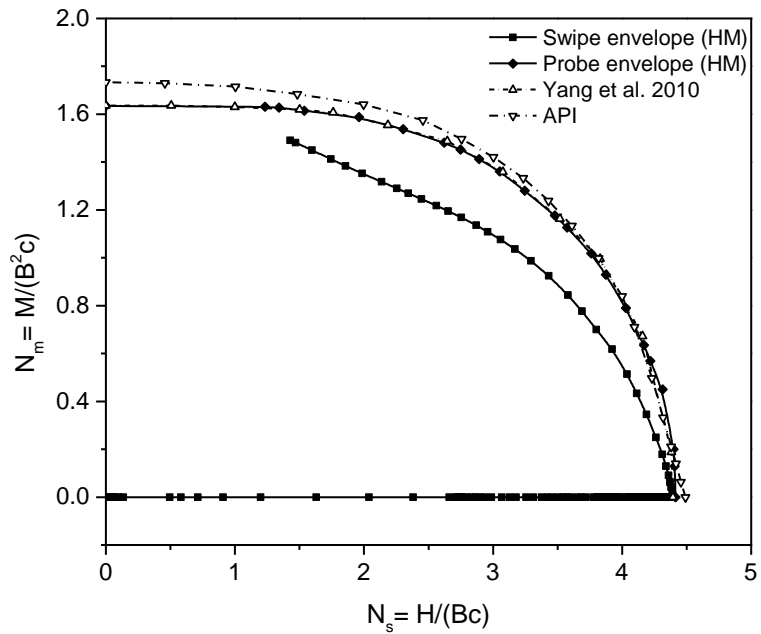


Figure 5: Compares between the failure envelope for swipe and probe tests at H-M plane

Additionally, it also compares the failure envelope found from both swipe and probe analysis. Failure envelope of swipe test lies inside the true failure envelope. If the anchor is brought to sliding failure first, and then rotated at a fixed horizontal position, the resulting load path lies significantly inside the true failure envelope (Gourvenec & Randolph, 2003).

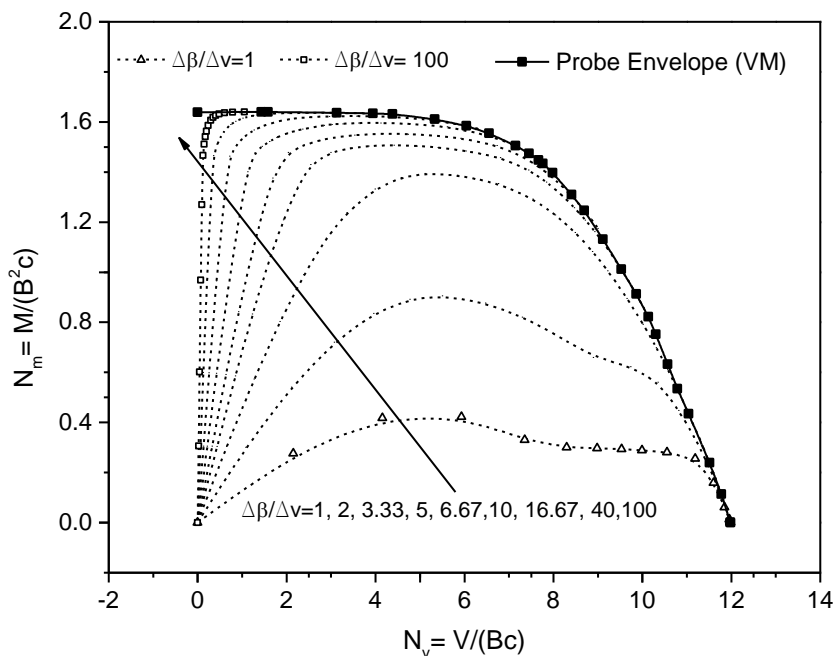


Figure 6: Loading path and failure envelope at V-M plane (H=0)

Symmetry of the problem indicates that $f(M,H) = f(M,-H)$, $f(V,H) = f(V,-H)$ and $f(V,M) = f(V,-M)$, so that only positive load combinations of HM, VH and VM are required to define the complete failure envelope. The Figure.4 also represents the prove of symmetry of HM loading. For this reason, further analyses were carried out only with the positive load combinations. The Figure.5 represents the failure loci under VM loading. To construct

complete failure envelope ten probe tests ($\Delta\beta/\Delta v$) ranging from 1 to 100 are carried out as shown in Fig.6 . All probes are shown by dotted lines. It also proves that after reaching a failure all loading path travel along the failure envelope. At a lower normal loading upto $0.5V_{ult}$, moment reduces slightly and after that it changes sharply. Hence, it can be concluded that, when normal force $>0.5V_{ult}$ then vertical loading dominates the failure mechanism.

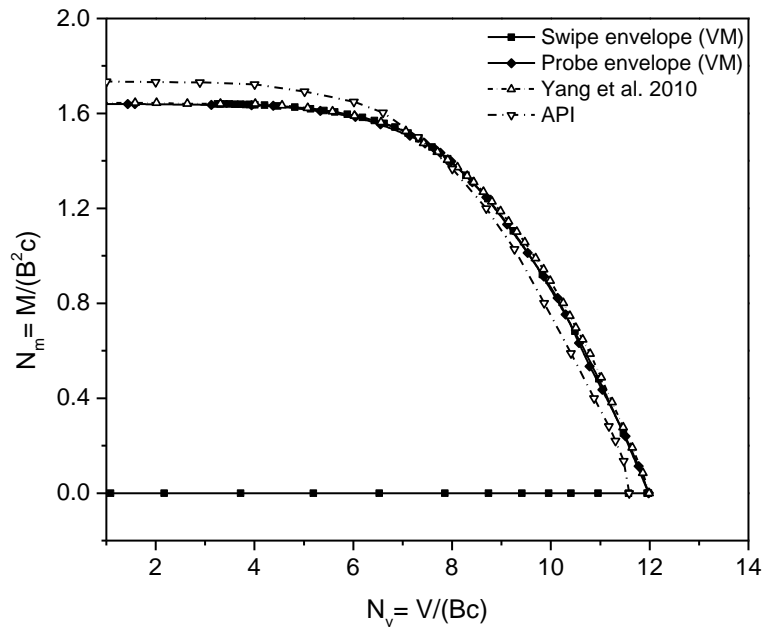


Figure 7: Compares between the failure envelope for swipec and probe tests at V-M plane

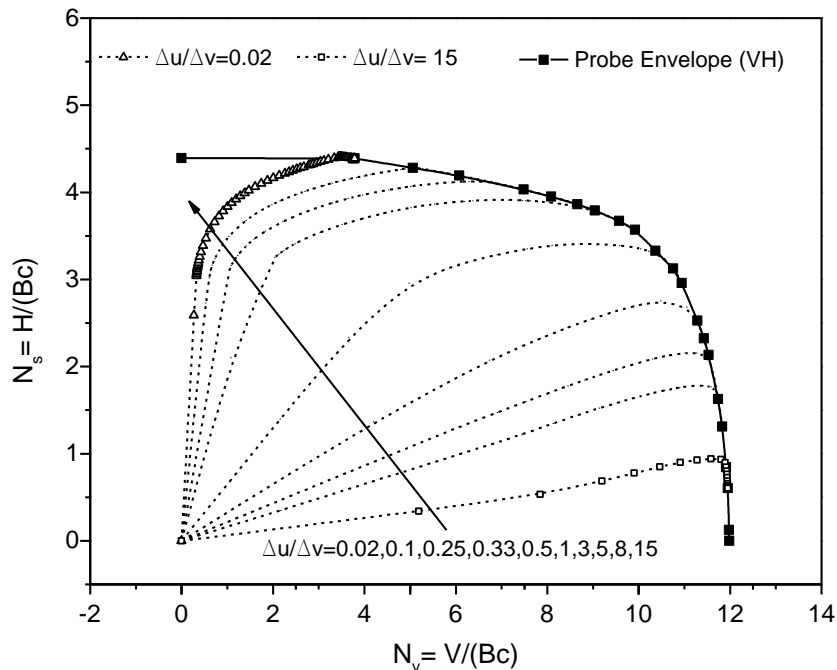


Figure 8: Loading path and failure envelope at V-H plane (M=0)

This trend found same in Andersen et al. (2003) and Yang et al. (2010) studies, as shown in Figure.7. Figure.7 also shows a good agreement of probe and swipec test in VM plane. Fig.8 represents the interaction diagram in horizontal and vertical loading plane (VH). In this study,

in order to construct complete interaction diagram, 9 probe tests were carried out. The H:V interaction curves as shown in Figure.8. The Figure.8 drop abruptly at large values of N_v implying that parallel loading has little impact on the normal capacity before it reaches $0.5H_{ult}$. In this case, normal load dominates the failure mechanism. Figure.9 shows the compares between the swipe and probe test. In the case of VH loadings, swipe envelope lies slightly inside the probe envelope. It also agreed well with the research conducted by Andersen et al. (2003) and Yang et al. (2010).

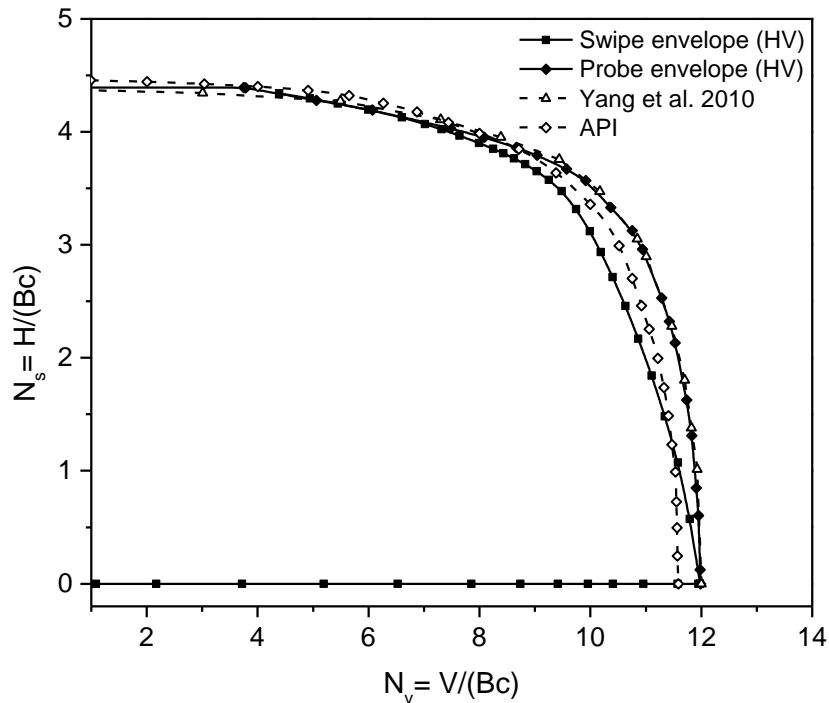


Figure 9: Compares between the failure envelope for swipe and probe tests at V-H plane

3.1 Soil failure mechanism

Soil failure mechanism under combined loading is illustrated in Figure.10 by equivalent plastic strain (ϵ_p) and the deformed soil shape is calculated by load-displacement probe test in HM plane. This method consists of two steps. In first step a load (say horizontal load, H) is applied directly along the horizontal direction by the load-controlled method which is less than the ultimate failure load (H_{ult}) and a failure point is gained on the failure envelope. In its second step, horizontal load along this direction is kept constant and rotational displacement is applied until the rotational failure occurs in that direction. A point, at which load value in horizontal direction can be predefined, is probed on the envelope in HM failure plane. Figure.10a represents the failure mechanism in fully bonded condition under pure shear loading. It demonstrates that, the maximum plastic strain occurs along the side of the plate. The black triangles left and right side of the plate are soil wedges that move rigidly as plate progresses and finally the plastic strain contours travel around the plate. Figure.10b represents the failure mechanism in fully bonded condition under pure vertical loading. The white rectangle is the plate anchor which is modelled as a rigid plate. The plastic yielding region of the soil progresses similarly on each side of the plate anchor such that substantial portions of soil are involved.

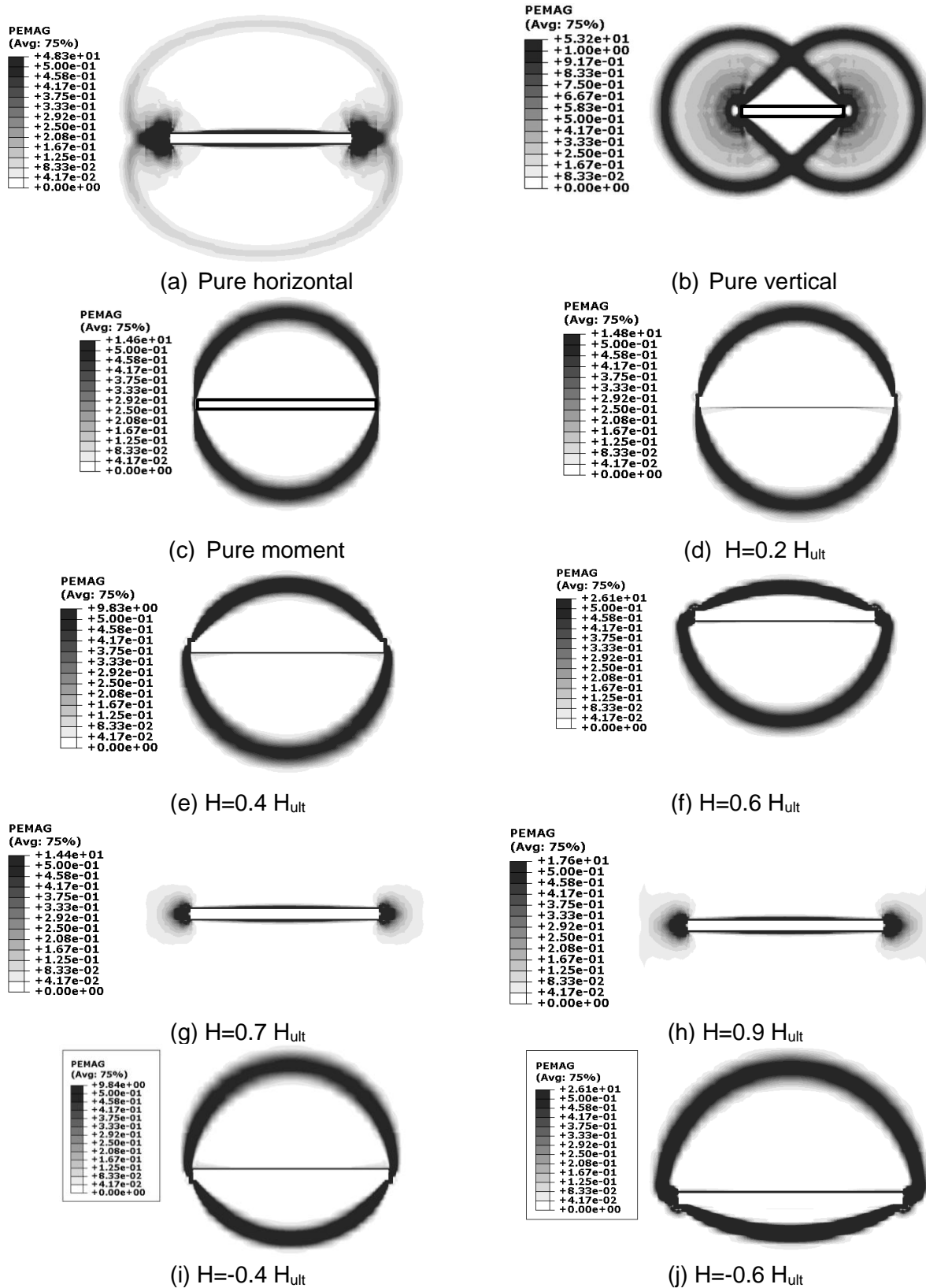


Figure 10: Distribution of plastic strain (ϵ_p) under combined loading.

It also shows the plastic strain where the soil is “flowing” around the plate anchor as two symmetrical circles, demonstrating a complete plastic failure mechanism has formed as the critical load is reached. The white triangles on each side of the plate are soil wedges that

move basically rigidly with the plate as it progresses. It also indicates that, the maximum plastic strain occurs along the sides of the “rigid” soil wedges (Andersen et al., 2003 and Yang et al., 2010). This is closely in consensus with classical theory. Fig.10c represents the plastic strain flow at failure under pure rotation. It illustrates that, the plastic strain start to flow along the edge of anchor and travel symmetrically. The maximum plastic strain occurs as two half circles at top and bottom of the anchor plate.

For the case of HM load combination, Figure.10d through Figure.10h represents the failure mechanism in positive HM loadings (H=left to right positive and M=clockwise positive) and Figure.10i and Figure.10j shows the failure mechanism in-HM loadings. When $H=0.2 H_{ult}$, soil flows symmetrically around the plate as two half circles. As the horizontal load increases, upper half circles starts to diminishing and in that case horizontal loading dominates the failure mechanism. When $H>0.7 H_{ult}$, then circular zone does not exist and soil starts yielding due to the horizontal loading. Plastic strain distribution of Figure.10i and Figure.10j are same as Figure.10e and Figure.10f, but reverse in direction, where, lower half circles starts to diminishing and in that case horizontal loading also dominates the failure mechanism. Hence, the total works done and ultimate failure load is same in both cases.

4. CONCLUSION

The drag anchor response under combined uni-directional horizontal, vertical and moment loadings are explored for strip horizontal anchor by FEA. In order to hypothesis the failure envelope in HM, VM and HV plane, both the swipe and probe tests were conducted. Additionally, to understand the failure mechanism in HM loading condition load-displacement probe tests were also conducted. Compared with the result of swipe and existing numerical studies it can be concluded that the probe test gives the correct prediction of the failure envelope in all loading plane. Result also reveals that the soil failure changes from symmetrical circular pattern to asymmetrical pattern due to the increase of horizontal load in HM plane.

REFERENCES

- Andersen, K. H., Murff, J. D., & Randolph, M. F. (2003). “Deepwater anchor design practice-vertically loaded drag anchors.” *Phase II Report to API/Deepstar, Norwegian Geotechnical Institute, Norway, Offshore Technology Research Center, USA and Centre for Offshore Foundation Systems, Australia.*
- Bransby, M. F., & Randolph, M. F. (1997). “Shallow foundations subject to combined loadings.” *In 9th International Conference of the International Association for Computer Methods and Advances in Geomec, (Vol. 3, pp. 1947–1952.*
- Bransby, M. F. & Randolph, M. F. (1998). “Combined loading of skirted foundations.” *Geotechnique, 48(5), 637–655.*
- Butterfield R, Houlsby GT, G. G. (1997). “Standardized sign conventions and notation for generally loaded foundations.” *Geotechnique, 47(5), 1051–4.*
- Cassidy, M. J., Byrne, B. W., & Houlsby, G. T. (2002). “Modelling the behaviour of circular footings under combined loading on loose carbonate sand.” 705–712.
- Cassidy, M. J., Randolph, M. F., and Wong, P. . (2012). “A plasticity model to assess the keying of plate anchors.” *Géotechnique, 62(9), 825.*
- Tian, Y., Gaudin, C., Cassidy, M. J., & Randolph, M. F. (2012). “Considerations on the Design of Keying Flap of Plate Anchors.” (2013). *Journal of Geotechnical and Geoenvironmental Engineering, 139(7), 1156–1164.*
- Elkhatib, S. (2006). *The behaviour of drag-in plate anchors in soft cohesive soils.* (Ph.D. thesis), University of Western Australia, Australia.
- Elkhatib, S., and Randolph, M. F. (2005). “The effect of interface friction on the performance of drag-in plate anchors.” Perth, Western Australia: Taylor & Francis., pp.171-177.

- Gourvenec, S. & Randolph, M. F. (2003). "Effect of strength non-homogeneity on the shape and failure envelopes for combined loading of strip and circular foundations on clay." *Geotechnique*, 53(6), 575–586.
- Houlsby, G. T. (1994). "Physical and numerical modelling of offshore foundations under combined loads." (*Doctoral dissertation, University of Oxford*).
- Kim, B. M. (2007). *Upper bound analysis for drag anchors in soft clay*. (Ph.D. thesis), Texas A&M University.
- Liu, J., Lu, L., and Hu, Y. (2016). "Keying behavior of gravity installed plate anchor in clay." *Ocean Engineering*, 114, 10–24.
- M P O'Neill, M F Bransby, and M F Randolph. (2003). "Drag anchor fluke-soil interaction in clays." *Canadian Geotechnical Journal*, 40(1), 78–94.
- Martin, C. M., & Houlsby, G. T. (2001). "Combined loading of spudcan foundations on clay: numerical modelling." *Géotechnique*, 51(8), 687–700.
- Nouri, H., Biscontin, G., and Aubeny, C. P. (2017). "Numerical prediction of undrained response of plate anchors under combined translation and torsion." *Computers and Geotechnics*, 81, 39–48.
- Aubeny, C. P., Murff, J. D., & Kim, B. M. (2008). "Prediction of Anchor Trajectory During Drag Embedment In Soft Clay." (2008). *International Journal of Offshore and Polar Engineering*, 18(4).
- Randolph, M. F., Gaudin, C., Gourvenec, S. M., White, D. J., Boylan, N., and Cassidy, M. J. (2011). "Recent advances in offshore geotechnics for deep water oil and gas developments." *Ocean Eng.*, 38(7), 818–834.
- Rowe, R. K. (1978). "Soil structure interaction analysis and its application to the prediction of anchor plate behaviour." (*Doctoral dissertation*).
- Song, Z., Hu, Y., & Randolph, M. F. (2008). "Numerical Simulation of Vertical Pullout of Plate Anchors in Clay." *Journal of Geotechnical and Geoenvironmental Engineering*, 134(6), 866–875.
- Song, Z., and Hu, Y. (2005). "Vertical pullout behaviour of plate anchors in uniform clay." Perth, Western Australia: Taylor & Francis.
- Wang, D., Hu, Y., & Randolph, M. F. (2009). "Three-Dimensional Large Deformation Finite-Element Analysis of Plate Anchors in Uniform Clay." (2010). *Journal of Geotechnical and Geoenvironmental Engineering*, 136(2), 355–365.
- Merifield, R. S., Lyamin, A. V., Sloan, S. W., & Yu, H. S. (2003) "Three-Dimensional Lower Bound Solutions for Stability of Plate Anchors in Clay." (2003). *Journal of Geotechnical and Geoenvironmental Engineering*, 129(3), 243–253.
- Wei, Q., Cassidy, M. J., Tian, Y., and Gaudin, C. (2015). "Incorporating Shank Resistance into Prediction of the Keying Behavior of Suction Embedded Plate Anchors." *Journal of Geotechnical and Geoenvironmental Engineering*, 141(1), 4014080.
- Yang, M., Murff, J. D., & Aubeny, C. P. (2010). "Undrained capacity of plate anchors under general loading." *Journal of geotechnical and geoenvironmental engineering*, 136(10), 1383–1393.